Available online at www.sciencedirect.com
SCIENCE DIRECT®
Journal of Molecular Structure 689 (2004) 199–212
Journal of MOLECULAR STRUCTURE
www.elsevier.com/locate/molstruc

Matrix isolation FT-IR spectroscopy and molecular orbital study of sarcosine methyl ester

A. Gómez-Zavaglia[a,b], R. Fausto[a,*]

[a]*Department of Chemistry, University of Coimbra, Coimbra P-3004-535, Portugal*
[b]*Facultad de Farmacia y Bioquímica, Universidad de Buenos Aires, RA-1113, Argentina*

Received 20 August 2003; revised 16 October 2003; accepted 16 October 2003

Abstract

N-methylglycine methyl ester (sarcosine-Me) has been studied by matrix isolation FT-IR spectroscopy and molecular orbital calculations undertaken at the DFT/B3LYP and MP2 levels of theory with the 6-311++G(d,p) and 6-31++G(d,p) basis set, respectively. Twelve different conformers were located in the potential energy surface of the studied compound, with the *ASC* conformer being the ground conformational state. This form is analogous to the dimethylglycine methyl ester most stable conformer and is characterized by a NH···O= intramolecular hydrogen bond; in this form, the ester group assumes the *cis* configuration and the O=C–C–N and *Lp*-N–C–C (where *Lp* is the nitrogen lone electron pair) dihedral angles are ca. −17.8 and 171.3°, respectively. The second most stable conformer (*GSC*) differs from the *ASC* conformer essentially in the conformation assumed by the methylamino group, which in this case is *gauche* (*Lp*-N–C–C dihedral angle equal to 79.4°). On the other hand, the third most stable conformer (*AAC*) differs from the most stable form in the conformation of the O=C–C–N axis (151.4°). These three forms were predicted to differ in energy by less than ca. 5 kJ mol^{-1} and represent ≈95% of the total conformational population at room temperature. FT-IR spectra were obtained for sarcosine-Me isolated in argon matrices ($T = 9$ K) revealing the presence in the matrices of the three lowest energy conformers predicted by the calculations. The matrices were prepared by deposition of the vapour of the compound using two different nozzle temperatures, 25 and 60 °C. The relative populations of the three conformers trapped in the matrices were found to be consistent with occurrence of conformational cooling during matrix deposition and with a stabilization of the most polar *GSC* and *AAC* conformers in the matrices compared to the gas phase. Indeed, like it was previously observed for the methyl ester of dimethylglycine [Phys. Chem. Chem. Phys. 5 (2003) 52] the different strength of the interactions between the conformers and the matrix environment seem to lead to a change in the relative order of stabilities of *GSC* and *ASC* upon going from the gas phase to the matrices, with the first conformer becoming the conformational ground state in the latter media. The assignment of the bands observed in the matrix spectra to the three experimentally observed conformers of sarcosine-Me is presented and discussed.

Keywords: *N*-methylglycine methyl ester; Conformers; Matrix isolation FT-IR spectroscopy; DFT calculations

1. Introduction

Alkyl esters derived from simple amino acids, in particular glycine and its *N*-methyl substituted derivatives, have important functions in different domains. For example, *N,N*-dimethylglycine (DMG) esters were recently proposed as new derivatives for the rapid, sensitive and selective analysis of primary and secondary alcohols in complex mixtures, by electronspray ionization tandem mass spectrometry (ESI-MS/MS) [1], while glycine and *N*-methylglycine (sarcosine) methyl esters have been shown to modulate the activity of pancreatic enzymes such as the transglutaminase, by regulating the cross-bridging of proteins [2,3]. Another important function of this family of compounds is that they are a source for lipid synthesis. Sarcosine esters, in particular, have been used in a large number of cosmetic formulations, as hair-conditioning and surfactant–cleaning agents [4]. Despite the practical relevance of this kind of compounds, they have been scarcely studied hitherto.

In previous recent studies [5–7], we have investigated DMG, DMG methyl ester and sarcosine isolated in low temperature inert gas matrices by FT-IR spectroscopy. The analysis of the experimental data was supported by extensive quantum chemical calculations, undertaken at

* Corresponding author.
E-mail address: rfausto@ci.uc.pt (R. Fausto).

0022-2860/$ - see front matter © 2003 Elsevier B.V. All rights reserved.
doi:10.1016/j.molstruc.2003.10.039

both DFT and MP2 levels of theory. In those studies, the structures and spectral signatures of the lowest energy conformers of the neutral monomeric compounds were characterized for the first time. In the case of DMG, the relatively strong OH···N intramolecular hydrogen bond that can be established between the carboxylic and amino groups was shown to assume a fundamental role in determining its most stable conformational state. Indeed, for that compound, the conformational ground state was found to be an intramolecularly O–H···N hydrogen-bonded conformer ($G'AT$), where the carboxylic acid group must assume the intrinsically less stable *trans* configuration in order to permit the establishment of the intramolecular hydrogen bond [5]. In the remaining experimentally observed conformers of DMG, the carboxylic moiety assumes the usual (most stable) *cis* conformation, while the N–C–C=O axis adopts preferentially the *syn* arrangement and the conformation around the N–C bond is either *anti* or *gauche* (*ASC* and *GSC* forms, respectively). In sarcosine, the presence of the amino hydrogen atom (which is absent in DMG) leads to stabilizing not only the *ASC* conformer (which in this case become the most stable form), but also the *GSC* conformer, due to the involvement of this atom in the establishment of an NH···O= intramolecular hydrogen bond in these two conformers. In sarcosine, the O–H···N hydrogen-bond does still lead to stabilization of conformers with the *trans* carboxylic group configuration but, in this case, this stabilization is not enough to make any of these forms more stable than the *ASC* conformer. Indeed, the energy difference between the most stable of the *trans* conformers ($G'AT$) and the conformational ground state (*ASC*) was found to be ca. 2 kJ mol^{-1}, which is nearly equal to the energy difference between *GSC* and *ASC* [7].

In the case of sarcosine-Me, the NH···O= hydrogen bond can be expected to be the dominant intramolecular interaction, since the OH···N hydrogen bond cannot be established due to the replacement of the carboxylic hydrogen atom by the methyl ester group. This interaction can take place in both the *ASC* and *GSC* conformers and it can then be easily anticipated that these two forms should be the ones with most relevant practical significance. These two conformers are also similar to those experimentally observed for the methyl ester of DMG [6], a compound that was found to present a particularly interesting conformational behaviour, being a notable example of a molecule where the relative stability of the two most stable conformers shows an inversion in going from the gaseous phase to the matrix isolated species [6]. This observation further stimulated us to look at the conformational properties of similar compounds. Hence, in the continuation of our studies on glycine-based compounds [5–9], the investigation of the conformational properties of sarcosine-Me appears to be of particular relevance. Following the same lines of our previous studies on glycine-based compounds, this article presents a combined matrix isolation FT-IR and theoretical study on sarcosine-Me.

2. Materials and methods

2.1. Computational methodology

The quantum chemical calculations were performed with GAUSSIAN 98 [10] at the DFT and MP2 levels of theory, using the 6-311++G(d,p) and 6-31++G(d,p) basis sets [11], respectively. The DFT calculations were carried out with the three-parameter density functional abbreviated as B3LYP, which includes Becke's gradient exchange correction [12], the Lee, Yang, Parr correlation functional [13] and the Vosko, Wilk and Nusair correlation functional [14].

Conformations were optimized at each level of theory using the Geometry Direct Inversion of the Invariant Subspace (GDIIS) method [15]. Vibrational frequencies were calculated at the DFT level and the corresponding Hessian matrices were used to check the nature of the critical points resulting from the optimisation procedure. All optimised structures were confirmed to be minimum energy conformations. The calculated frequencies were scaled down by a single factor (0.978) to correct them for the effects of basis set limitations, neglected part of electron correlation and anharmonicity effects, and were used to assist the analysis of the experimental spectra. Normal coordinates analyses were undertaken in the internal coordinates space as described by Schachtschneider [16] using the program BALGA and the optimised geometries and harmonic force constants resulting from the DFT(B3LYP)/6-311++G(d,p) calculations. Potential energy profiles for internal rotation were calculated performing a relaxed scan on the Potential Energy Surface (PES) of sarcosine-Me along the reaction coordinates and the transition state structures for conformational interconversions obtained using the Synchronous Transit-Guided Quasi-Newton (STQN) method [17].

2.2. Infrared spectroscopy

Sarcosine-Me was synthesized from sarcosine (Aldrich, purity 99%), following a procedure similar to those described in Refs. [18–20].

The IR spectra were collected on a Mattson (Infinity 60AR Series) Fourier Transform infrared spectrometer equipped with a deuterated triglycine sulphate (DTGS) detector and a Ge/KBr beamsplitter, with 0.5 cm^{-1} spectral resolution.

In the matrix isolation experiments, a glass vacuum system and standard manometric procedures were used to deposit the matrix gas (argon N60, obtained from Air Liquid). Matrices were prepared by co-deposition onto a cooled CsI substrate of the matrix gas and sarcosine-Me placed in a specially designed doubly termostatable Knudsen cell with shut-off possibility, whose main component is a NUPRO SS4BMRG needle valve. The temperature of the cell can be controlled separately in the valve nozzle and the sample compartment, enabling a more

precise control of the saturated gas pressure over the liquid sarcosine-Me and a better metering function of the valve. Further details of the experimental set up can be found in Ref. [21]. All experiments were done on the basis of an APD Cryogenics close-cycle helium refrigeration system with a DE-202A expander. The deposition temperature used was 9 K. Necessary modifications of the sample compartment of the spectrometer were made in order to accommodate the cryostat head and allow efficient purging of the instrument by a stream of dry air to remove water and CO_2 vapours. After depositing the compound, annealing experiments were performed until a temperature of 30 K.

3. Results and discussion

3.1. Molecular geometries and energies

Sarcosine-Me has three different internal rotation axes that can give rise to conformational isomers (*Lp*-N–C–C, N–C–C=O and O=C–O–C; *Lp* = lone electron pair of nitrogen atom). All of its possible conformations belong to the C_1 symmetry point group. The molecule possesses a chyral nitrogen atom and, for each one of the two spectroscopically (and energetically) equivalent arrangements around the nitrogen atom, sarcosine-Me may exist in 12 different conformational states, as predicted by systematic search on the potential energy surface of this molecule undertaken at the DFT(B3LYP)/6-311++G(d,p) and MP2/6-31++G(d,p) levels of theory.

At both levels of theory, the lowest energy conformers of sarcosine-Me exhibit a *cis* carboxylic ester group (O=C–O–C dihedral equal to 0°). All conformers presenting the *trans* ester configuration (O=C–O–C axis equal to 180°) correspond to high energy forms, with relative energies to the conformational ground state larger than 35 kJ mol^{-1}. The calculated relative energies (and dipole moments) of all the possible conformers of sarcosine-Me are presented in Table 1, while the calculated geometries and rotational constants for the three most stable conformers (*ASC*, *GSC* and *AAC*; see Fig. 1) are given in Table 2.[1]

According to the theoretical predictions, the conformational ground state of sarcosine-Me corresponds to the *ASC* conformer, where the N–C–C=O and *Lp*-N–C–C (*Lp* = lone electron pair) dihedral angles are −17.8° and 171.3°, respectively. The second most stable conformer according to the DFT calculations, *GSC*, differs from the most stable conformer in the *Lp*-N–C–C axis, which assumes a *gauche* (79.4°) configuration. These two conformers differ in energy only by ca. 1 kJ mol^{-1} and are similar to the first and third most stable conformers of the parent sarcosine molecule (the second most stable conformer of sarcosine has an OH···N intramolecular hydrogen bond that cannot have any counterpart in sarcosine-Me due to the OH substitution by the OCH_3 ester group). The third most stable conformer of sarcosine-Me (*AAC*; see Fig. 1) differs essentially from the *ASC* form in the conformation of the N–C–C=O axis (in *AAC*, this axis assumes approximately the *anti* configuration: 151.4°), being 4.74 kJ mol^{-1} higher in energy than this latter form.

Table 1
Relative energies (ΔE_{ZPE}), including zero point vibrational contributions and dipole moments (μ), for the various conformers of sarcosine-Me

Conformer	ΔE_{ZPE}		μ	
	DFT/B3LYP	MP2[a]	DFT	MP2
ASC	0.0 (−953104.597)[b]	0.0 (−950103.84)[b]	1.65	1.75
GSC	1.01	3.13	1.87	1.83
AAC	4.74	2.96	2.32	2.27
GAC	6.14	6.44	2.48	2.51
G′SC	8.80	8.41	2.31	2.34
G′AC	12.59	12.86	1.91	1.55
AST	33.52	35.46	3.67	3.60
GST	33.74	38.48	4.48	4.57
G′AT	38.68	39.46	4.79	4.66
GAT	40.26	39.30	4.53	4.56
G′ST	44.16	47.45	5.18	5.22
AAT	47.44	47.48	4.00	3.89

Energies in kJ mol^{-1}; Dipole moments in Debyes; conformers are depicted in Fig. 1.
[a] Zero point energy corrections taken from DFT(B3LYP)/6-311++G(d,p) calculations.
[b] Total energies with zero point vibrational energy contribution in parenthesis.

The MP2 calculations yield slightly different results, in particular in what concerns the relative energies of conformers *GSC* and *AAC* (see Table 1). The most relevant difference in the intramolecular interactions present in the two conformers is the absence in *GSC* of the $NCH_3\cdots O$ steric repulsion (which is present in both *AAC* and *ASC*). Accordingly, the C1–C9–N4 angle, which is a good measure of the strength of the $NCH_3\cdots O$ repulsion, is considerably smaller in *GSC* than in *ASC* and *AAC* (by 5° and 8°, respectively, see Table 2). It is then possible to attribute to a more repulsive MP2 $NCH_3\cdots O$ potential the observed differences between the two methods of calculation. This conclusion should, however, been taken with care, since the basis set employed in this study for the MP2 calculations was smaller than that used for the DFT calculations and, therefore, part of the effect may also be attributed to this factor.

Using the Boltzmann distribution and the predicted (DFT)[2] relative conformational energies to estimate the populations of the different conformers of sarcosine-Me at room temperature (298 K), the most stable conformer can be expected to account for 52% of the total population, *GSC* for 34% and *AAC* for 8%, with the remaining nine forms having

[1] Calculated geometries and rotational constants for the higher energy conformers are available from the corresponding author upon request.

[2] Using MP2 relative energies the predicted populations at room temperature are (*ASC*:*GSC*:*AAC*)(59%:17%:18%).

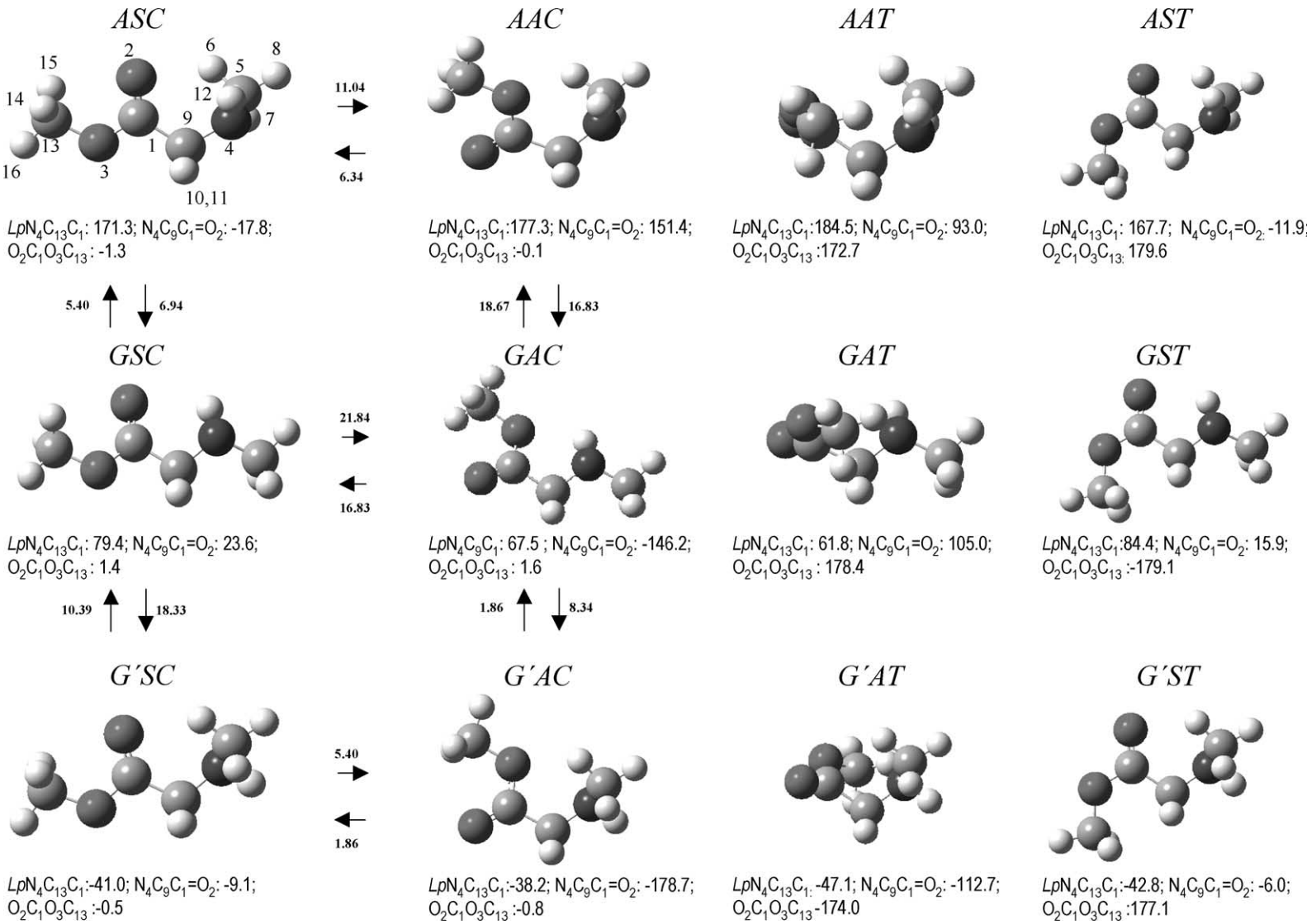

Fig. 1. Conformers of sarcosine-Me with atom numbering scheme and energy barriers (kJ mol^{-1}) for conformational interconversion between *cis* carboxylic ester conformers. For convenience, the values of the most relevant dihedral angles (degrees) are included.

Table 2
Optimised geometries for the most stable conformers of sarcosine methyl ester

Parameter	*ASC*		*GSC*		*AAC*	
	DFT/B3LYP	MP2	DFT/B3LYP	MP2	DFT/B3LYP	MP2
Bond lengths (pm)						
$C_1{=}O_2$	120.7	122.3	120.7	122.3	120.6	122.3
$C_1{-}O_3$	134.8	135.5	134.6	135.3	135.0	135.8
$C_1{-}C_9$	153.0	152.3	151.4	151.0	153.2	152.4
$O_3{-}C_{13}$	144.2	144.6	144.1	144.6	144.1	144.5
$N_4{-}C_5$	146.3	146.3	145.6	145.8	146.1	146.1
$N_4{-}C_9$	144.6	144.8	144.8	145.1	144.9	145.1
$N_4{-}H_{12}$	101.4	101.5	101.4	101.6	101.3	101.5
$C_5{-}H_6$	109.4	109.0	109.4	109.0	109.2	108.9
$C_5{-}H_7$	110.0	109.6	110.4	109.9	109.4	109.0
$C_5{-}H_8$	109.2	108.8	109.2	108.8	110.2	109.8
$C_9{-}H_{10}$	109.3	109.1	110.9	110.4	109.3	109.0
$C_9{-}H_{11}$	109.7	109.3	109.4	109.1	109.6	109.3
$C_{13}{-}H_{14}$	108.8	108.4	109.1	108.7	109.1	108.7
$C_{13}{-}H_{15}$	109.1	108.7	108.8	108.4	109.1	108.7
$C_{13}{-}H_{16}$	109.1	108.7	109.1	108.7	108.8	108.4
Bond angles (degrees)						
$O_2{=}C_1{-}O_3$	123.8	123.9	123.9	124.1	123.5	123.6
$O_2{=}C_1{-}C_9$	125.0	124.7	124.8	124.5	124.6	125.3
$C_1{-}O_3{-}C_{13}$	116.3	114.7	116.1	114.5	116.1	114.5
$C_5{-}N_4{-}C_9$	114.3	112.6	113.8	112.2	114.4	112.6
$N_4{-}C_5{-}H_6$	109.2	108.6	109.8	109.1	109.2	109.0
$N_4{-}C_5{-}H_7$	114.2	113.9	109.4	113.5	109.3	108.7
$N_4{-}C_5{-}H_8$	109.1	108.9	109.4	109.2	114.3	113.9
$H_6{-}C_5{-}H_7$	108.4	108.8	107.6	108.1	107.6	108.1
$H_6{-}C_5{-}H_8$	109.1	108.0	107.5	108.0	108.2	108.5
$N_4{-}C_9{-}H_{10}$	110.0	109.6	113.5	113.5	109.9	109.5
$N_4{-}C_9{-}H_{11}$	109.7	109.7	110.9	110.3	109.1	109.1
$C_9{-}N_4{-}H_{12}$	109.6	108.8	109.4	108.6	110.1	109.3
$H_{10}{-}C_9{-}H_{11}$	106.1	107.0	106.3	107.1	106.5	107.6
$C_1{-}C_9{-}N_4$	115.4	114.5	110.8	109.9	118.3	116.4
$C_1{-}C_9{-}H_{10}$	108.8	108.9	105.9	106.5	106.5	106.8
$C_1{-}C_9{-}H_{11}$	106.4	106.8	109.2	109.4	106.0	107.0
$N_4{-}C_9{-}H_{10}$	110.0	109.6	113.5	113.5	109.9	109.5
$O_3{-}C_{13}{-}H_{14}$	105.5	105.0	110.4	110.1	110.4	110.0
$O_3{-}C_{13}{-}H_{15}$	110.4	110.1	105.4	104.9	110.4	110.1
$O_3{-}C_{13}{-}H_{16}$	110.4	110.1	110.4	110.0	105.6	105.0
Dihedral angles (degree)						
$O_2{=}C_1{-}O_3{-}C_{13}$	1.3	−1.7	1.4	1.3	−0.1	−0.2
$N_4{-}C_9{-}C_1{=}O_2$	−17.7	−23.0	23.6	29.6	151.4	144.5
$O_2{=}C_1{-}C_9{-}H_{10}$	−141.9	−146.1	−99.9	−93.7	27.3	21.8
$O_2{=}C_1{-}C_9{-}H_{11}$	104.2	98.6	146.0	150.9	−85.9	−93.2
$C_9{-}N_4{-}C_5{-}H_6$	−63.5	−64.2	−65.1	−64.7	−62.5	−63.1
$C_9{-}N_4{-}C_5{-}H_7$	58.1	57.2	55.7	55.9	180.0	179.2
$C_9{-}N_4{-}C_5{-}H_8$	179.3	178.4	177.1	177.4	58.7	57.9
$C_5{-}N_4{-}C_9{-}C_1$	−70.6	−67.3	−163.6	−166.3	−65.3	−60.9
$C_9{-}C_1{-}O_3{-}C_{13}$	176.7	176.2	−176.5	−176.4	−177.8	−178.1
$C_1{-}O_3{-}C_{13}{-}H_{14}$	−179.8	−179.2	60.2	59.8	−60.0	−60.2
$C_1{-}O_3{-}C_{13}{-}H_{15}$	−60.2	−59.6	179.8	179.4	60.7	60.6
$C_1{-}O_3{-}C_{13}{-}H_{16}$	60.6	61.3	−60.7	−61.1	−179.7	−179.8
Rotational constants (MHz)						
A	6433.4807	6167.1599	8780.8179	8594.1376	4355.6517	4318.5939
B	1412.0828	1451.2519	1235.7246	1247.4360	1747.5011	1787.7761
C	1323.6369	1368.5822	1114.5208	1124.3102	1459.7343	1517.9239

See Fig. 1 for atom numbering.

a joint population of ca. 6%. At 333 K (the second temperature of the valve nozzle used in the matrix isolation experiments), the estimated populations of the most stable conformers change to: 49% for the *ASC*, 34% for *GSC* and 9% for *AAC*. The three most stable conformers are then predicted to account for 94% of the population at room temperature and 92%, at 333 K (Fig. 2). Hence, only these conformers appear to be of practical interest and might be expected to be observed experimentally with the techniques used in this study.

Having located all minima on the sarcosine-Me potential energy surface, an effort was made to calculate the potential energy profile for all possible interconversions between the *cis* carboxylic ester conformers. The transition state structures were obtained using the Synchronous Transit-Guided Quasi-Newton (STQN) method [17] and the interconversion reaction coordinates correspond essentially to internal rotations around the C–N central bond and/or the C–C bond. The results are shown in Figs. 3 and 4. There are several energy barriers that are predicted by the calculations to be relatively low (≤ 7 kJ mol^{-1}). For example, the predicted *GSC* → *ASC* direct and inverse barriers (which involve a rotation around the *Lp*-N–C–C axis) are 5.40 and 6.94 kJ mol^{-1}, respectively, and the *AAC* → *ASC* barrier

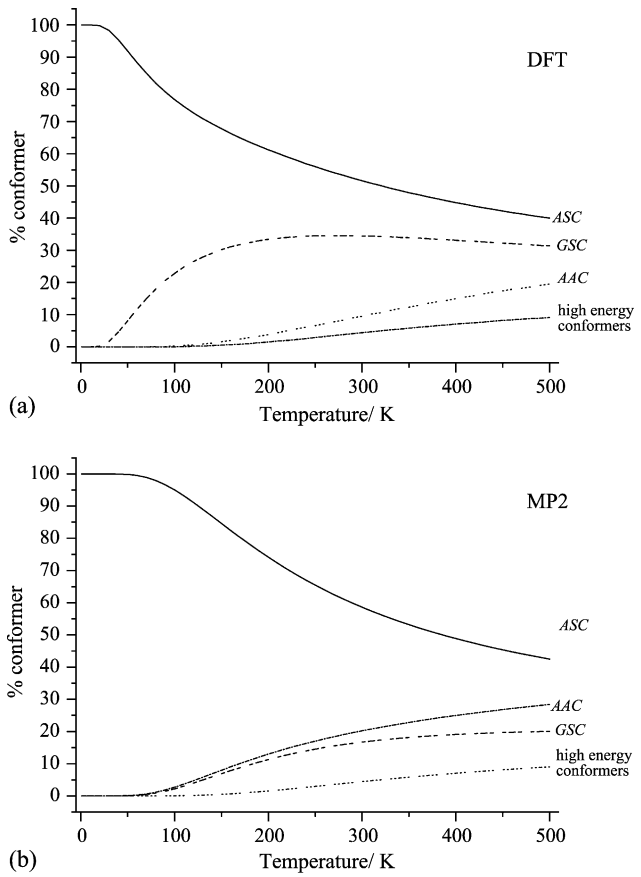

Fig. 2. Population of the different conformers of sarcosine-Me upon the range 0–500 K, assuming the Boltzmann distribution and using the (a) DFT and (b) MP2 predicted relative conformational energies.

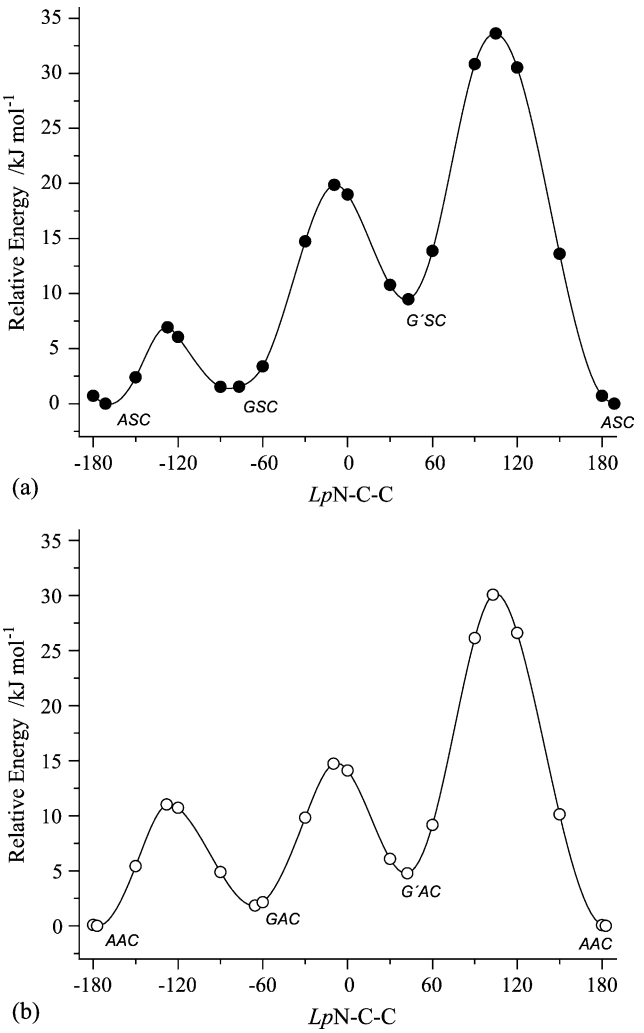

Fig. 3. DFT(B3LYP)/6-311++G(d,p) calculated potential energy profile for internal rotation around the N_4–C_9 bond. (a) *ASC* ↔ *GSC* ↔ *G′SC* interconversion path (-●-) (b) *AAC* ↔ *GAC* ↔ *G′AC* interconversion path (-○-).

(which involves change in the conformation of the O=C–C–N axis) is 6.34 kJ mol^{-1}, being in both cases, similar to the corresponding barriers found for sarcosine [7].

3.2. Vibrational spectra

The infrared spectra of sarcosine-Me isolated in argon matrices (substrate temperature: 9 K) obtained using two different nozzle temperatures (298 and 333 K) are presented in Fig. 5. The calculated (DFT) spectra for the three most stable conformers of sarcosine-Me are also plotted in this figure, using as weighting factors for intensities the estimated relative conformational populations resulting from the DFT calculations. The definition of the symmetry coordinates selected to perform the normal mode analysis and the potential energy distribution results obtained from those calculations are presented in Tables 3–6, together with the proposed assignments for the experimental bands.

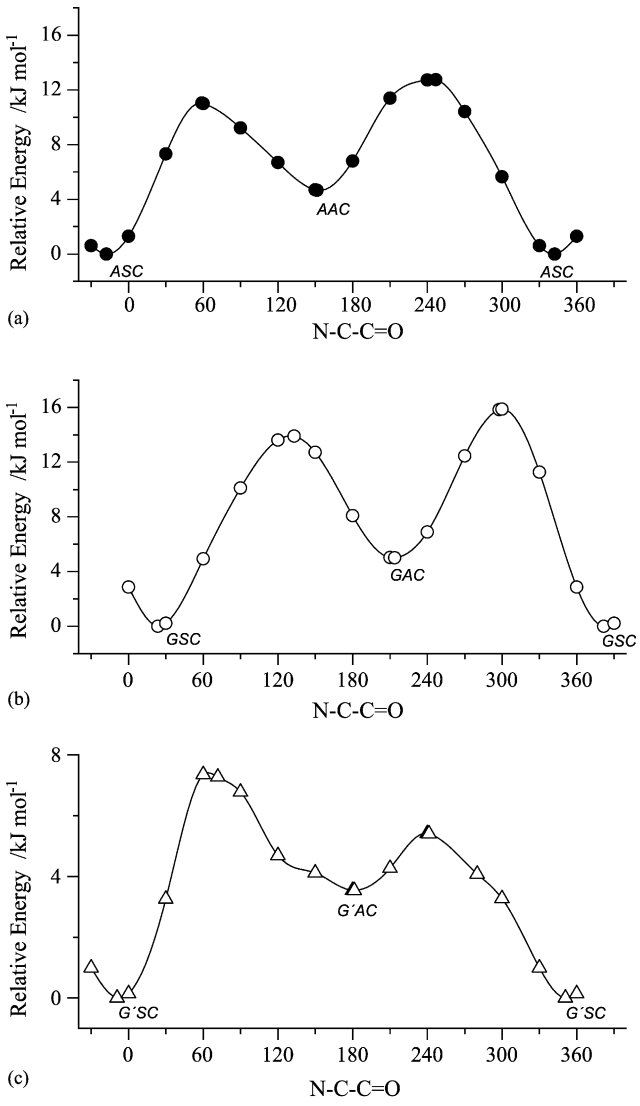

Fig. 4. DFT(B3LYP)/6-311++G(d,p) calculated potential energy profile for internal rotation around the C_1–C_9 bond. (a) *ASC* ↔ *AAC* (-●-); (b) *GSC* ↔ *GAC* (-○-) and (c) *G′SC* ↔ *G′AC* (-△-) interconversion paths.

According to the results, the three most stable conformers predicted by the calculations (*ASC*, *GSC* and *AAC*) contribute to the observed spectra. The interpretation of the experimental results was facilitated by the good general agreement between the calculated and observed spectra. The assignment of the bands to the individual conformers was also supported by their dependence with the temperature of the valve nozzle. Upon increasing the temperature of the nozzle, the bands due to the *ASC* conformer reduce of intensity, while those ascribable to the *GSC* and *AAC* conformers increase (see Fig. 5). Hence, in consonance with the theoretical predictions, the matrix isolation infrared results clearly indicate that, in the gaseous phase, the *ASC* conformer is the ground conformational state.

In the carbonyl stretching region (νC=O; Fig. 5A) the calculations predicted bands at 1750.8, 1754.2 and 1749.9 cm^{-1}, for *ASC*, *GSC* and *AAC*, respectively. The bands observed at 1764.7 and 1751.8 cm^{-1}, which show a strong decrease of intensity upon increasing the temperature of the nozzle, are ascribed to the νC=O mode of the *ASC* conformer in Fermi resonance with the first overtone of the νC–C vibration (whose fundamental is observed at 882.9 cm^{-1}). On the other hand, the doublets at 1758.0/1755.8 cm^{-1} and 1742.1/1736.8 cm^{-1}, which increase of intensity with the nozzle temperature, are assigned to the *GSC* and *AAC* conformers, respectively.

The nature of the splitting effects observed in the carbonyl stretching region for the different conformers deserve here a further comment. The splitting is clearly larger in *ASC* (12.9 cm^{-1}) than in *GSC* and *AAC* (2.2 and 5.6 cm^{-1}, respectively), indicating that, in this case, it must have a different origin. As mentioned above, for *ASC* we attribute the observed splitting to a Fermi resonance interaction with the first overtone of the νC–C vibration. Taking the average frequency of the two components of the doublet as reference value, the anharmonicity of the νC–C mode can be roughly estimated as being 7.6 cm^{-1}. Considering that the experience is that cubic force constants, responsible for Fermi interactions, are not very conformer-sensitive, it is easy to conclude that the same phenomenon cannot operate in *GSC* and *AAC*. In fact, the corrected by anharmonicity frequencies of the first overtone of the νC–C mode in the latter conformers are ca. 1784 and 1626 cm^{-1}, for *GSC* and *AAC*, which are, respectively, too high and low to interact significantly with the corresponding carbonyl stretching vibrations. Hence, for these two conformers it is likely that the splitting results from matrix site effects. Indeed, the magnitude of the observed splittings is consistent with this interpretation. We cannot also exclude the possibility of occurrence of site splitting for *ASC*, but the complex profile of the spectral region under analysis and the relatively larger bandwidths of the bands due to this form preclude a definitive answer to this question. Anharmonic frequency calculations could eventually be useful to give further support to the proposed interpretation.

The most intense bands in the 950–1240 cm^{-1} range are those corresponding to the νC–O and νCN stretching vibrations (Fig. 5B). According to the calculations, the bands corresponding to the νC–O mode of the two most stable conformers should appear at 1192.2 cm^{-1} (*ASC*) and 1213.4 cm^{-1} (*GSC*). In the experimental spectra, the band at 1195.6 cm^{-1}, which corresponds to the most intense band in the experimental spectrum obtained at 298 K, is then ascribed to the νC–O mode of *ASC*. As expected, this band considerably decreases its intensity in the spectrum obtained with the nozzle valve at 333 K, whereas the band at 1220.7 cm^{-1} (attributed to the same mode in the *GSC* conformer) increases of intensity. The νC–O vibration in *AAC* is predicted to occur at 1220.6 cm^{-1} and is assigned to the shoulder observed at 1225.3 cm^{-1}.

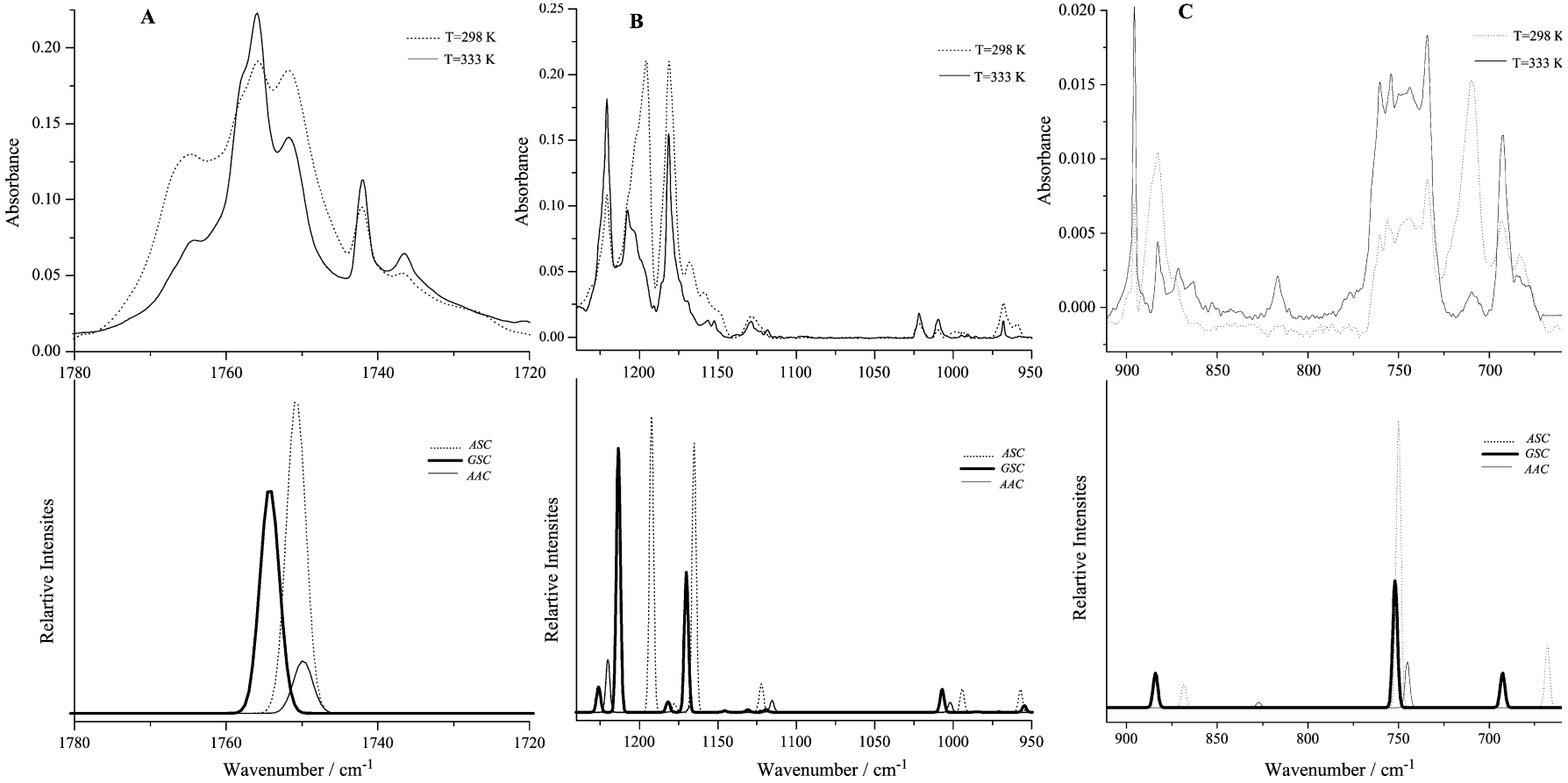

Fig. 5. Comparison of the experimental infrared spectra of sarcosine-Me trapped in an argon matrix using two different nozzle temperatures (- - -298 K; – 333 K), and the DFT(B3LYP)/6-311++G(d,p) calculated spectra for *ASC* (···), *GSC* (▬) and *AAC* (—) conformers. (A) carbonyl stretching spectral range; (B) 1240–950 cm^{-1} spectral range; (C) 910–660 cm^{-1} spectral range. In the theoretical spectra, the calculated integral intensities were weighted by the relative populations of the different conformers at 298 K using the DFT calculated energies.

Table 3
Definition of symmetry coordinates

	Definition	Approximate description
S_1	$\nu(C_1-O_2)$	$\nu C{=}O$
S_2	$\nu(C_1-O_3)$	$\nu C-O$
S_3	$\nu(O_3-C_{13})$	$\nu O-C$
S_4	$\nu(C_1-C_9)$	$\nu C-C$
S_5	$\nu(C_9-H_{10})+\nu(C_9-H_{11})$	νCH_2 s
S_6	$\nu(C_9-H_{10})-\nu(C_9-H_{11})$	νCH_2 as
S_7	$\nu(C_9-N_4)$	$\nu C-N$
S_8	$\nu(N_4-C_5)$	$\nu N-C$
S_9	$\nu(N_4-H_{12})$	$\nu N-H$
S_{10}	$\nu(C_5-H_7)+\nu(C_5-H_6)+\nu(C_5-H_8)$	νCH_3s
S_{11}	$2\nu(C_5-H_7)-\nu(C_5-H_6)-\nu(C_5-H_8)$	νCH_3as′
S_{12}	$\nu(C_5-H_6)-\nu(C_5-H_8)$	νCH_3as″
S_{13}	$\nu(C_{13}-H_{14})+\nu(C_{13}-H_{15})+\nu(C_{13}-H_{16})$	νCH_3s
S_{14}	$2\nu(C_{13}-H_{14})-\nu(C_{13}-H_{15})-\nu(C_{13}-H_{16})$	νCH_3as′
S_{15}	$\nu(C_{13}-H_{15})-\nu(C_{13}-H_{16})$	νCH_3as″
S_{16}	$\delta(C_1-O_3-C_{13})$	δCOC
S_{17}	$2\delta(O_2-C_1-O_3)-\delta(C_9-C_1-O_2)-\delta(C_9-C_1-O_3)$	δOCO
S_{18}	$\delta(C_9-C_1-O_2)-\delta(C_9-C_1-O_3)$	$\delta C-C{=}O$
S_{19}	$5(H_{10}-C_9-H_{11})-\delta(H_{10}-C_9-C_1)-\delta(H_{11}-C_9-C_1)-\delta(H_{10}-C_9-N_4)-\delta(H_{11}-C_9-N_4)-\delta(N_4-C_9-C_1)$	δCH_2
S_{20}	$-\delta(H_{10}-C_9-C_1)-\delta(H_{11}-C_9-C_1)-\delta(H_{10}-C_9-N_4)-\delta(H_{11}-C_9-N_4)+4\delta(N_4-C_9-C_1)$	δNCC
S_{21}	$\delta(H_{10}-C_9-C_1)+\delta(H_{11}-C_9-C_1)-\delta(H_{10}-C_9-N_4)-\delta(H_{11}-C_9-N_4)$	ωCH_2
S_{22}	$\delta(H_{10}-C_9-C_1)-\delta(H_{11}-C_9-C_1)-\delta(H_{10}-C_9-N_4)+\delta(H_{11}-C_9-N_4)$	$twCH_2$
S_{23}	$\delta(H_{10}-C_9-C_1)-\delta(H_{11}-C_9-C_1)+\delta(H_{10}-C_9-N_4)-\delta(H_{11}-C_9-N_4)$	γCH_2
S_{24}	$2\delta(C_5-N_4-C_9)-\delta(C_5-N_4-H_{12})-\delta(H_{12}-N_4-C_9)$	δCNC
S_{25}	$\delta(C_5-N_4-H_{12})-\delta(C_5-N_4-C_9)$	δNH
S_{26}	$\delta(H_6C_5H_8)+\delta(H_8C_5H_6)+\delta(H_7C_5H_6)-\delta(H_7C_5N_4)-\delta(H_8C_5N_4)-\delta(H_6C_5N_4)$	δCH_3s
S_{27}	$2\delta(H_7C_5H_8)-\delta(H_8C_5H_6)-\delta(H_7C_5H_6)$	δCH_3as′
S_{28}	$\delta(H_8C_5H_6)-\delta(H_7C_5H_6)$	δCH_3as″
S_{29}	$2\delta(H_6C_5N_4)-\delta(H_8C_5N_4)-\delta(H_7C_5N_4)$	$\gamma CH_3'$
S_{30}	$\delta(H_8C_5N_4)-\delta(H_6C_5N_4)$	$\gamma CH_3''$
S_{31}	$\delta(H_{15}C_{13}H_{16})+\delta(H_{16}C_{13}H_{14})+\delta(H_{15}C_{13}H_{14})-\delta(H_{15}C_{13}O_3)-\delta(H_{16}C_{13}O_3)-\delta(H_{14}C_{13}O_3)$	δCH_3s
S_{32}	$2\delta(H_{15}C_{13}H_{16})-\delta(H_{16}C_{13}H_{14})-\delta(H_{15}C_{13}H_{14})$	δCH_3as′
S_{33}	$\delta(H_{16}C_{13}H_{14})-\delta(H_{15}C_{13}H_{14})$	δCH_3as″
S_{34}	$2\delta(H_{14}C_{13}O_3)-\delta(H_{16}C_{13}O_3)-\delta(H_{15}C_{13}O_3)$	$\gamma CH_3'$
S_{35}	$\delta(H_{16}C_{13}O_3)-\delta(H_{15}C_{13}O_3)$	$\gamma CH_3''$
S_{36}	$\tau(C_9-C_1-O_3-C_{13})$	$\tau C-O$
S_{37}	$\tau(N_4-C_9-C_1=O_2)$	$\tau C-C$
S_{38}	$\tau(C_1-C_9-N_4-C_5)$	$\tau C-N$
S_{39}	$\tau(C_9-N_4-C_5-H_7)$	τNC
S_{40}	$\tau(H_{14}-C_{13}-O_3-C_1)$	$\tau C-O$
S_{41}	O_2 out of plane $C_9-C_1-O_3$	$\gamma C{=}O$
S_{42}	Inversion	Inversion

ν, bond stretching, δ, bending, γ rocking, ω, wagging, tw, twisting, τ, torsion.

The νCN stretching mode is predicted to have similar frequencies in all the observable conformers (see Tables 4–6). Accordingly, we assign this vibration in the three conformers to the intense band observed at 1181.1 cm^{-1}. This band slightly decreases of intensity upon increasing the temperature of the nozzle due to the larger expected contribution of the *ASC* conformer to its total intensity.

The bands corresponding to the νO–C stretching vibration are predicted to appear at 994.3, 1007.1 and 1009.6 cm^{-1} for *ASC*, *GSC* and *AAC*, respectively, and could be expected to give rise to well separated bands in the experimental spectra. This circumstance, as well as the fact that the intensity of this mode predicted by the calculations to be larger for the less stable conformers, makes the study of this spectral region particularly interesting for identification of bands due to the individual forms and further analyses. Indeed, the νO–C bands originated in *ASC*, *GSC* and *AAC* are clearly observed as well separated bands at ca. 997 (triplet of bands resulting from matrix site splitting), 1021.9 and 1009.6 cm^{-1}, respectively (see Fig. 5B).

It is interesting that the features assigned to νO–C in *ASC* occur as a well separated triplet, while for the other two conformers singlets (or very nearly so) are observed. This indicates that the O–C stretch in *ASC* shows a much higher site sensitivity than in the other two conformers. This is consistent with the fact that this vibration was found to be considerably more delocalized in *ASC* than in *GSC* and *AAC*. In fact, the PED contribution associated with

Table 4
Experimental band assignment and calculated [DFT (B3LYP)/6-311++G(d,p)] wavenumbers and intensities, and normal coordinate analysis for sarcosine methyl ester (*ASC* conformer)[a]

Approximate Description	Experimental		Calculated		PED[d]
	Wavenumber	Intensity[b]	Wavenumber (Scaled 0.978)	Intensity[c]	
νN-H			3457.8	2.4	S_9(99.0)
$\nu CH_3as'$	3075.1	1.0	3088.4	7.1	S_{14}(97.5)
$\nu CH_3as''$	3031.0	3.7	3055.8	9.9	S_{15}(100.0)
$\nu CH_3as''$	3006.0	8.2	3029.6	15.0	S_{12}(89.4)
νCH_2 as	2995.3	6.3	3011.2	4.4	S_5(15.7) + S_6(84.2)
$\nu CH_3as'$	2962.3	24.8	2985.6	18.0	S_{10}(29.2)+S_{11}(60.3)+S_{12}(10.4)
νCH_3s			2984.3	16.5	S_{13}(97.4)
νCH_2 s	2947.5	10.8	2960.1	10.4	S_5(84.1)+S_6(15.7)
νCH_3s	2918.0/2911.6/2895.7/ 2884.5/2879.2	7.4/8.0/9.4/ 9.4/9.6	2907.2	35.3	S_{10}(66.3)+S_{11}(33.6)
νC=O	1764.7/1751.8	51.3/72.8	1750.8	120.7	S_1(88.3)
δNH	1485.6	3.9	1493.6	6.8	S_{25}(40.5)+S_{28}(42.6)+S_{30}(12.2)
$\delta CH_3as''$	1470.8	3.5	1470.5	1.0	S_{25}(42.4)+S_{28}(47.4)
$\delta CH_3as'$	1462.6	17.6	1464.6	5.1	S_{32}(81.9)+S_{34}(10.0)
$\delta CH_3as'$	1455.6	10.0	1457.3	5.4	S_{27}(89.3)
$\delta CH_3as''$	1449.4	22.3	1451.5	5.1	S_{33}(91.7)
δCH_3s	1439.1	28.8	1437.0	3.8	S_{31}(78.9)
δCH_3s	1410.5/ 1405.5	2.2/2.5	1430.6	5.4	S_{19}(39.7)+S_{26}(46.7)
δCH_2	1388.8	5.1	1417.6	3.8	S_{19}(51.5)+S_{26}(46.4)
ωCH_2	1311.6	2.7	1338.9	5.4	S_{21}(77.6)
$twCH_2$	1289.3	7.8	1282.1	3.9	S_{22}(61.2)+S_{30}(15.3)
νC-O	1202.6/ 1195.6	59.9/82.8	1192.2	9.8	S_2(32.0)+S_{34}(24.1)
$\gamma CH_3'$	1181.1	82.6	1177.6	2.6	S_7(20.3)+S_{34}(38.7)
νC-N	1181.1/ 1168.0/1158.6	82.6/22.7/13.7	1165.1	114.9	S_2(15.9)+S_7(17.4)+S_{17}(10.5)+S_{34}(15.5)
$\gamma CH_3''$	1148.5	8.0	1144.5	0.7	S_{35}(90.7)
$\gamma CH_3'$	1128.8/1126.1/1122.6	6.7/5.9/3.7	1123.3	2.8	S_{29}(76.2)
νN-C			1122.0	9.0	S_7(13.8)+S_8(28.4)+S_{22}(17.4)+ S_{30}(17.2)
νO-C	999.0/997.1/994.0	2.0/2.0/2.2	994.3	9.1	S_3(39.1)+S_8(10.0)+S_{30}(17.7)
$\gamma CH_3''$	968.0/959.2	10.6/4.3	957.2	8.9	S_3(41.2)+S_{23}(16.6)+S_{30}(15.4)
γCH_2	939.4/936.6	0.8/1.0	926.1	5.0	S_7(10.7)+S_8(35.6)+S_{23}(25.6)+S_{41}(14.2)
νC-C	886.3/882.9/873.6	3.7/4.5/1.2	868.4	5.0	S_2(22.7)+S_4(26.6)
inversion	709.8	6.5	750.0	61.5	S_7(10.4)+S_{24}(11.7)+S_{42}(41.0)
δOCO	683.4	1.8	668.0	13.3	S_4(13.6)+S_{17}(23.5)+S_{20}(11.3)+S_{24}(10.4) +S_{42}(11.6)
γC=O	575.6	1.6	566.4	5.1	S_{23}(20.9)+S_{41}(67.0)
δCNC			459.4	1.7	S_4(19.5)+S_{18}(11.3)+S_{20}(10.9)+S_{24}(20.4)
δC-C=O			358.8	2.0	S_{16}(22.0)+S_{18}(25.0)+S_{24}(23.7)
δCOC			305.1	15.6	S_{16}(23.8)+S_{17}(17.3)+S_{20}(18.4)+S_{39}(11.2) +S_{42}(9.6)
τNC	n.i.		237.9	0.5	S_{16}(19.3)+S_{18}(19.9)+S_{39}(46.7)
τC-O			177.2	3.1	S_{20}(12.8)+S_{36}(51.5)
δNCC			165.7	2.5	S_{18}(12.5)+S_{20}(16.3)+S_{36}(21.7)+S_{39}(26.2)
τC-O			127.9	0.6	S_{38}(11.0)+S_{40}(81.6)
τC-C			101.1	0.7	S_{36}(21.4)+S_{38}(66.3)
τC-N			49.4	0.6	S_{37}(95.7)

[a] Wavenumbers in cm^{-1}, calculated intensities in km mol^{-1}. Experimental normalized intensities (I^{exp}) were calculated using the formula: $I_i^{exp} = A_i^{exp} \frac{\sum I^{calc}(x) \times p_{298\ K}(x)}{\sum A^{exp}}$; where x designates conformers *ASC*, *GSC* and *AAC*, $p_{298\ K}$ the population factor at $T = 298$ K, calculated on the basis of relative energies predicted by DFT calculations, A^{exp} is the experimentally measured absorbance, and the sums extend to all three conformers and all bands observed (in the denominator of the fraction) or which have an experimental counterpart (in the numerator). n.i., non-investigated. ν, bond stretching, δ, bending, γ rocking, tw, twisting, ω, wagging, τ, torsion, s, symmetric, as, asymmetric. See Table 3 for definition of coordinates.

[b] Note that several bands are assigned to more than one conformer and in these cases the intensity of the band is reported only once in Tables 4–6.

[c] Calculated intensities (I^{calc}; km mol^{-1}) were weighted by the population factor ($T = 298$ K) for the *ASC* conformer as predicted by the DFT calculations taking into consideration the calculated relative conformational energies (0.514).

[d] Only PED values greater than 10% are given.

the stretching of the O–C bond is only 39% (Table 4), while in *GSC* and *AAC* it amounts, respectively, to 49 and 74% (Tables 5 and 6). Furthermore, in the former conformer, the normal mode has a substantial (18% PED) contribution from a methyl rocking coordinate, while in both *GSC* and *AAC*, besides the dominant coordinate, only the νC–C of νC–C and νN–C stretching coordinates are involved significantly (ca. 10%) in the vibrational mode (see Tables 4–6). It seems reasonable to consider that a more delocalized coordinate, also involving

Table 5
Experimental band assignment and calculated [DFT (B3LYP)/6-311++G(d,p)] wavenumbers and intensities, and normal coordinate analysis for sarcosine methyl ester (*GSC* conformer)[a]

Approximate Description	Experimental		Calculated		PED[d]
	Wavenumber	Intensity[b]	Wavenumber (Scaled 0.978)	Intensity[c]	
νN-H			3459.5	5.0	S_9(99.2)
$\nu CH_3as'$	3075.1		3089.8	4.6	S_{14}(97.4)
$\nu CH_3as''$	3036.3		3057.0	6.3	S_{15}(99.9)
$\nu CH_3as'$	3006.0		3030.8	9.5	S_{11}(88.3)
νCH_2 as	2985.9	5.9	2989.6	5.1	S_5(44.4)+S_6(54.1)
νCH_3s	2962.3		2985.1	10.4	S_{13}(96.1)
$\nu CH_3as''$			2978.6	14.4	S_{10}(41.5)+S_{12}(58.4)
νCH_3s	2863.0/2859.3/2854.2/2849.5	9.6/9.6/9.2/9.6	2863.1	40.1	S_{10}(52.3)+S_{11}(11.8)+S_{12}(36.1)
νCH_2 s	2806.3/2798.3	9.4/10.8	2825.4	23.0	S_5(55.0)+S_6(45.2)
νC=O	1758.0/1755.8	63.8/75.3	1754.2	87.0	S_1(87.6)
$\delta CH_3as'$	1478.7	2.9	1485.3	6.8	S_{25}(29.9)+S_{27}(49.1)
δNH	1476.2	2.3	1474.2	0.4	S_{19}(21.5)+S_{25}(25.3)+S_{27}(25.7)
$\delta CH_3as'$	1462.6		1464.9	3.6	S_{32}(81.5)+S_{34}(10.1)
$\delta CH_3as''$			1455.6	2.0	S_{19}(19.0)+S_{25}(16.4)+S_{28}(49.3)
δCH_2	1449.4		1453.8	5.2	S_{19}(52.2)+S_{28}(33.8)
$\delta CH_3as''$			1451.1	3.5	S_{33}(93.1)
δCH_3s	1439.1		1438.6	7.3	S_{31}(83.9)
δCH_3s	1416.3/1413.9	1.8/1.6	1426.9	1.1	S_{26}(91.0)
ωCH_2	1358.7/1340.3	8.4/2.2	1355.0	20.4	S_{21}(57.1)+S_{25}(9.6)
$twCH_2$	1225.3		1226.0	9.8	S_{22}(62.9)
νC-O	1225.3/1220.7/1207.5	24.5/42.5/53.8	1213.4	102.1	S_2(33.2)
$\gamma CH_3'$	1181.1		1181.7	4.1	S_7(9.6)+S_{34}(57.6)
νC-N			1170.0	53.8	S_2(10.2)+S_7(20.6)+S_{22}(10.9) +S_{34}(14.0)
$\gamma CH_3''$	1148.5		1145.6	0.6	S_{35}(91.4)
νN-C			1130.9	1.0	S_8(41.0)+S_{30}(18.5)
$\gamma CH_3''$	1118.4	1.4	1119.2	1.1	S_{29}(24.8)+S_{30}(44.9)
νO-C	1021.9	4.5	1007.1	8.8	S_3(48.6)+S_4(9.7)+S_8(13.2)
γCH_2	985.3	0.2	985.1	0.2	S_{23}(67.1)+S_{41}(19.0)
$\gamma CH_3'$	968.0		954.7	2.6	S_3(25.2)+S_7(17.5)+S_8(11.4)+S_{29}(15.3)
νC-C	895.7	3.1	884.0	7.5	S_2(25.2)+S_3(13.5)+S_4(20.6)
inversion	776.6/760.3/756.4/754.4 748.8/744.8/739.5/734.3	1.4/2.3/2.7/2.5 2.5/2.7/2.5/3.7	751.9	27.4	S_{24}(22.0)+S_{42}(47.2)
δOCO	693.2	2.7	692.7	7.5	S_4(10.6)+S_{17}(27.8)+S_{20}(12.3)+S_{42}(17.8)
γC=O	599.1	2.2	594.5	4.5	S_{23}(14.6)+S_{41}(65.4)
δC-C=O			417.2	1.1	S_{16}(12.7)+S_{18}(50.6)
δCNC			346.8	1.7	S_4(18.3)+S_{17}(11.5)+S_{20}(19.3)+S_{24}(24.8)+ S_{42}(11.4)
δCOC			298.6	5.5	S_{16}(52.0)+S_{17}(16.5)+S_{24}(11.5)
τNC			241.3	0.4	S_{39}(90.5)
τC-O	n.i.		191.6	1.3	S_{18}(11.4)+S_{20}(12.7)+S_{36}(50.2)
δNCC			152.3	0.7	S_{18}(10.7)+S_{20}(18.0)+S_{36}(25.1)+S_{37}(13.5) +S_{40}(15.1)
τC-O			121.7	0.3	S_{36}(15.6)+S_{40}(79.7)
τC-N			96.2	1.2	S_{37}(20.0)+S_{38}(67.4)
τC–C			63.7	0.6	S_{37}(65.4)+S_{38}(23.5)

[a] Wavenumbers in cm^{-1}, calculated intensities in km mol^{-1}. Experimental normalized intensities (I^{exp}) were calculated using the formula:; $I_i^{exp} = A_i^{exp} \frac{\sum I^{calc} \sum(x) \times p_{298\ K}(x)}{\sum A^{exp}}$; where x designates conformers *ASC*, *GSC* and *AAC*, $p_{298\ K}$ the population factor at $T = 298$ K, calculated on the basis of relative energies predicted by DFT calculations, A^{exp} is the experimentally measured absorbance, and the sums extend to all three conformers and all bands observed (in the denominator of the fraction) or which have an experimental counterpart (in the numerator). n.i., non-investigated. ν, bond stretching, δ, bending, γ rocking, tw, twisting, ω, wagging, τ, torsion, s, symmetric, as, asymmetric. See Table 3 for definition of coordinates.

[b] Only the intensities of the bands which are due either to conformer *GSC* exclusively or to both *GS* C and *AAC* are given.

[c] Calculated intensities (I^{calc}; km mol^{-1}) were weighted by the population factor ($T = 298$ K) for the *GSC* conformer as predicted by the DFT calculations taking into consideration the calculated relative conformational energies (0.345).

[d] Only PED values greater than 10% are given.

larger displacements of lighter atoms, should be more sensitive to differences in the local environment (matrix site), thus justifying the observations.

Finally, in the studied low frequency range, the bands corresponding to νC–C and amine inversion modes appear as the most prominent bands. The bands due to νC–C are observed at 895.7 cm^{-1} for *GSC*, 882.9 cm^{-1} for *ASC* and 816.6 cm^{-1} for *AAC* (Fig. 5C). The origin of the weak bands at 871.7 and 863.1 cm^{-1} is uncertain, but they must belong to either *GSC* or *AAC* (they increase with the nozzle temperature), with all probability corresponding to overtones or combination tones involving low frequency

Table 6
Experimental band assignment and calculated [DFT (B3LYP)/6-311++G(d,p)] wavenumbers and intensities, and normal coordinate analysis for sarcosine methyl ester (*AAC* conformer)[a]

Approximate Description	Experimental		Calculated		PED[d]
	Wavenumber	Intensity[b]	Wavenumber (Scaled 0.978)	Intensity[c]	
νN-H			3470.2	0.3	S_9(98.9)
νCH_3as´´	3075.1		3087.8	1.0	S_{14}(24.0)+S_{15}(73.7)
νCH_3as´	3036.3		3056.0	1.4	S_{14}(75.4)+S_{15}(24.6)
νCH_3as´´	3006.0		3029.8	2.1	S_{12}(92.4)
νCH_2 as			3020.4	0.7	S_5(16.1)+S_6(83.7)
νCH_3as´	2962.3		2985.6	1.9	S_{10}(36.6)+S_{11}(52.9)
νCH_3s			2984.4	3.2	S_{13}(94.4)
νCH_2 s	2947.5		2963.0	1.4	S_5(83.7)+S_6(16.2)
νCH_3s	2863.0/2859.3/ 2854.2/2849.5		2890.2	6.2	S_{10}(58.9)+S_{11}(41.2)
νC=O	1742.1/1736.5	37.6/20.5	1749.9	20.0	S_1(88.9)
δCH_3as´´			1490.6	1.2	S_{25}(38.3)+S_{28}(45.1)+S_{30}(12.6)
δNH	1462.2		1467.2	0.3	S_{25}(43.5)+S_{28}(44.0)
δCH_3as´´			1464.9	0.7	S_{32}(19.0)+S_{33}(60.4)
δCH_3as´	1455.6		1457.3	0.6	S_{27}(84.6)
δCH_3as´	1449.4		1450.6	0.7	S_{32}(70.0)+S_{33}(21.8)
δCH_3s	1439.1		1437.4	0.4	S_{31}(80.6)
δCH_2	1427.7	2.0	1430.1	0.6	S_{19}(44.6)+S_{26}(44.4)
δCH_3s			1419.5	0.1	S_{19}(45.5)+S_{26}(48.3)
ωCH_2	1330.0/1325.1	0.2/0.2	1324.5	0.8	S_{21}(91.9)
$twCH_2$			1289.4	1.6	S_{22}(67.4)+S_{30}(12.4)
νC-O	1220.7		1220.1	20.0	S_2(40.1)+S_4(16.3)+S_{17}(12.2)
γCH_3´´			1179.9	0.2	S_{34}(16.3)+S_{35}(50.4)
νC-N	1168.0		1167.8	2.1	S_7(33.6)+S_8(10.4)+S_{30}(13.9)
γCH_3´	1148.5		1145.5	0.1	S_{34}(69.9)+S_{35}(20.7)
γCH_3´			1122.7	0.7	S_{29}(81.2)
νN-C	1118.4		1115.4	4.4	S_7(12.7)+S_8(30.1)+S_{22}(13.9)+S_{30}(14.4)
νO-C	1009.6	2.5	1002.0	3.8	S_3(74.0)+S_4(10.4)
γCH_3´´	968.0		970.8	0.5	S_7(12.4)+S_8(10.4)+S_{23}(21.6)+S_{30}(28.8)
γCH_2	929.0	0.6	923.9	0.6	S_7(9.5)+S_8(34.1)+S_{23}(31.7)+S_{41}(16.2)
δCC	816.6	0.2	827.2	1.1	S_2(39.8)+S_4(14.3)+S_{17}(14.3)
inversion	776.6/760.3/756.4/ 754.4/748.8/744.8/ 739.5/734.3		745.1	9.8	S_7(14.4)+S_{42}(44.5)
δOCO	637.1	0.4	650.3	3.1	S_{17}(10.0)+S_{20}(13.5)+S_{23}(10.5)+S_{41}(15.5)+S_{42}(11.1)
γC=O	575.6		564.2	0.4	S_4(20.1)+S_{17}(15.2)+S_{23}(10.4)+S_{41}(41.7)
νNCC			488.0	0.3	S_4(16.5)+S_{18}(23.0)+S_{20}(13.3)+S_{24}(14.4)
δCNC			362.9	0.9	S_{16}(11.2)+S_{18}(20.5)+S_{24}(40.6)+S_{42}(14.5)
δCOC			308.8	1.3	S_{16}(45.1)+S_{20}(12.7)+S_{38}(13.1)
δC-C=O			235.5	0.0	S_{16}(13.4)+S_{18}(17.8)+S_{38}(37.5)+S_{39}(25.9)
τC-O	n.i.		188.8	0.5	S_{36}(60.9)+S_{38}(21.8)
τNC			164.0	0.1	S_{18}(15.0)+S_{20}(22.1)+S_{39}(72.4)+S_{42}(10.8)
τC-O			123.4	0.0	S_{40}(89.0)
τC-N			97.4	0.0	S_{20}(9.7)+S_{36}(30.1)+S_{38}(56.1)
τC–C			45.8	0.1	S_{37}(107.8)

[a] Wavenumbers in cm^{-1}, calculated intensities in km mol^{-1}. Experimental normalized intensities (I^{exp}) were calculated using the formula:; $I_i^{exp} = A_i^{exp} \frac{\sum I^{calc}(x) \times p_{298\ K}(x)}{\sum A^{exp}}$; where x designates conformers *ASC*, *GSC* and *AAC*, $p_{298\ K}$ the population factor at $T = 298$ K, calculated on the basis of relative energies predicted by DFT calculations, A^{exp} is the experimentally measured absorbance, and the sums extend to all four conformers and all bands observed (in the denominator of the fraction) or which have an experimental counterpart (in the numerator). w, weak, sh, shoulder, n.i., non-investigated. ν, bond stretching, δ, bending, γ rocking, tw, twisting, ω, wagging, τ, torsion, s, symmetric, as, asymmetric. See Table 3 for definition of coordinates.

[b] Only the intensities of the bands which are due to conformer *AAC* exclusively are given.

[c] Calculated intensities (I^{calc}; km mol^{-1}) were weighted by the population factor ($T = 298$ K) for the *AAC* conformer as predicted by the DFT calculations taking into consideration the calculated relative conformational energies (0.076).

[d] Only PED values greater than 10% are given.

fundamentals appearing below the lower frequency limit of our experimental set up. The amine inversion mode in both *GSC* and *AAC* forms is ascribed to the multiplet of bands observed at ca. 750 cm^{-1}, which increase with the nozzle temperature. In *ASC*, the band due to this mode is observed at 709.8 cm^{-1},separated from the inversion bands due to the other conformers, in spite of the theoretical calculations prediction that this vibration should give rise to bands at a similar frequency in all three conformers. However, the temperature dependence of the above-discussed

observed features strongly supports the proposed assignment (see Fig. 5C). Note that the amine inversion mode involves mainly the displacement of the amino hydrogen atom and is then essentially analogous to a NH bending vibration. In a similar way to what is commonly observed for the OH bending modes in carboxylic acid monomers isolated in argon matrices, this mode could then be expected to be strongly affected by site splitting. Indeed, despite site splitting effects are, strictly speaking, always unpredictable (a detailed knowledge of the characteristics of the matrix sites would be required to make reliable predictions of this property and of its dependence with the conformational state of the solute), thumb rules are that large amplitude flexible vibrational coordinates involving displacements of light atoms possessing a significant charge or more delocalised vibrations are usually more sensitive to matrix site effects. This is in consonance with the observed profile for the 750 cm^{-1} band, assigned to the inversion vibration of both *GSC* and *AAC* forms, and also justifies its comparative broadness.

Since for the methyl ester of DMG the relative stability of the conformers that are the analogous of the *ASC* and *GSC* forms of sarcosine-Me was found to be different in the gas phase and in the matrices [6], with the first being the most stable form in the gas and the second (and most polar form) the most stable conformer in the matrices, an estimation of the relative stability of the observed conformers of sarcosine-Me in the matrices was attempted. Taking the DFT results as reference data, the estimated populations (%) for *ASC*, *GSC* and *AAC*, at 298 and 333 K (nozzle temperatures) are, respectively, 52:34:8 and 49:34:9. If we neglect the existence of the high-energy conformers, these populations slightly change to 55:37:8 and 53:37:10. On the other hand, the estimated populations for the three conformers in the matrices prepared with the nozzle temperatures above, extracted from the observed intensities of the νO–C bands (which are well separated bands due to a single conformer) and using the predicted intensities as weighting factors, are 49:44:8 and 14:60:26. Hence, it can be concluded that in the matrices the population of the *ASC* conformer is smaller than that expected on the basis of theory, while those of *GSC* and *AAC* are larger. This is particularly evident in the case of the higher nozzle temperature experiment, where an unexpected low population of *ASC* was observed for the matrix isolated compound. It is obvious from these results that conformational cooling is taking place during deposition and different levels of interaction with the matrix are changing the relative energies of the conformers when compared with the gas phase. The dipole moments of both *GSC* (1.87 Debye) and *AAC* (2.32 Debye) are larger than that of *ASC* (1.65 Debye) and they are then expected to be stabilized in matrices compared with gas phase. Such stabilization of more polar isomers in matrices relatively to gas phase is a common phenomenon [6,22,23]. Indeed, the results now obtained for sarcosine-Me seem to indicate that for this molecule, like for DMG methyl ester [6], the *GSC* conformer is stabilized enough to become the most stable conformer in the matrices. Hence, during the landing of the molecules on the cold substrate, local heating effects due to dissipation of the energy available in the gaseous beam may enable conformational isomerization to take place, leading to an increased population of *GSC* at expenses of *ASC* comparatively to the gas phase. This effect was found to be relatively small when the gaseous beam is at room temperature (the predicted populations for the gas phase and those estimated in the matrix do not differ very much), but it is considerably more important when the temperature of the beam increases, as demonstrated by the large differences between the estimated populations of the conformers for the gas phase at 333 K and the observed populations in the corresponding matrix.

Annealing experiments (up to a temperature of 30 K) were also undertaken with the matrices prepared using the two nozzle temperatures, to check the possibility of conformational interconversion in the matrix isolated sarcosine-Me, *after* deposition. In both cases, no changes were observed that could be ascribed to conformer interconversion, indicating that the energy barriers are high enough to avoid these processes to take place. Indeed, during annealing, only the appearance of the characteristic bands of aggregated species [5,7] could be noticed, starting to be observed at a temperature of ca. 20 K.

4. Conclusion

According to DFT(B3LYP)/6-311++G(d,p) and MP2/6-31++G(d,p) calculations, the conformational ground state of gaseous sarcosine-Me is the intramolecularly N–H···O= hydrogen-bonded *ASC* form, where the O=C–O–C group assumes the *cis* configuration and the O=C–C–N and *Lp*-N–C–C (where *Lp* is the nitrogen lone electron pair) dihedral angles are ca. −17.8 and 171.3°, respectively. The second most stable conformer (*GSC*) differs to the *ASC* conformer in the *Lp*-N–C–C dihedral angle, being *gauche* in this case (79.4°). These two forms were predicted to differ in energy by less than ca. 1 kJ mol^{-1} and are predicted by the calculations to represent, together with the third most stable conformer *AAC*, ≈95% of the conformational population of the gas at room temperature.

Matrix isolated infrared spectroscopy allowed, for the first time, unequivocal observation of the three most stable conformers of sarcosine-Me predicted by the calculations and their vibrational characterization. Assignment of the observed spectra of the matrix isolated compound was carried out on the basis of their comparison with the theoretically predicted spectra for the *ASC*, *GSC* and *AAC* conformers and taking into consideration the changes observed due to the use of different experimental conditions. The experimental results indicate that in the matrix the *GSC*

conformer is the most stable conformer, while in consonance with the theoretical predictions the conformational ground state in the gas phase is *ASC*. These results closely follow data previously obtained for DMG methyl ester [6] and further demonstrate that, for molecules exhibiting different conformers with nearly the same energy, the different strengths of their interactions with the matrix may play a decisive role in defining the order of the conformational states.

Acknowledgements

This work was supported by the Portuguese Fundação para a Ciência e a Tecnologia (Research Project POCTI/-QUI/43366/2001 and Grant FCT #SFRH/BPD/11499/2002) and FEDER.

References

[1] D.W. Johnson, J. Mass. Spectrom. 36 (2001) 277.
[2] C. Alarcon, I. Valverde, W.J. Malaisse, Biosci. Rep. 5 (1985) 581.
[3] A. Sener, M.E. Dunlop, R. Gomis, P.C. Mathias, F. Malaisse-Lagae, W.J. Malaisse, Endocrinology 117 (1985) 237.
[4] R.S. Lanigan, Int. J. Toxicol. 20 (2001) 1.
[5] A. Gómez, A. Gómez, I. Zavaglia, R. Fausto, Phys. Chem. Chem. Phys. 5 (2003) 41.
[6] A. Gómez-Zavaglia, R. Fausto, Phys. Chem. Chem. Phys. 5 (2003) 52.
[7] A. Gómez-Zavaglia, R. Fausto, Vibrat. Spectrosc. (2003) in press.
[8] S.G. Stepanian, I.D. Reva, E.D. Radchenko, M.T.S. Rosado, M.L.T.S. Duarte, R. Fausto, L. Adamowicz, J. Phys. Chem. A 102 (1998) 1041.
[9] S.G. Stepanian, I.D. Reva, E.D. Radchenko, L. Adamowicz, J. Phys. Chem. A. 105 (2001) 664.
[10] M. Frisch, G. Trucks, H. Schlegel, G. Scuseria, M. Robb, J. Cheeseman, V. Zakrzewski, J. Montgomery, R. Stratmann, K. Burant, S. Dapprich, J. Millam, A. Daniels, K. Kudin, M. Strain, O. Farkas, J. Tomasi, V. Barone, M. Cossi, R. Cammi, B. Mennucci, C. Pomelli, C. Adamo, S. Clifford, J. Ochterski, G. Petersson, P. Ayala, Q. Cui, K. Morokuma, D. Malick, A. Rabuck, K. Raghavachari, J. Foresman, J. Cioslowski, J. Ortiz, A. Baboul, B. Stefanov, G. Liu, A. Liashenko, P. Piskorz, I. Komaromi, R. Gomperts, R. Martin, D. Fox, T. Keith, M. Al-Laham, C. Peng, A. Nanayakkara, M. Challacombe, P. Gill, B. Johnson W. Chen, M. Wong, J. Andres, C. Gonzalez, M. Head-Gordon, S. Replogle, J. Pople. 1998. GAUSSIAN 98, revision A.9; Gaussian Inc.: Pittsburgh, PA.
[11] M.J. Frisch, M. Head-Gordon, J.A. Pople, Chem. Phys. Lett. 166 (1990) 281.
[12] A.D. Becke, Phys. Rev. A 38 (1988) 3098.
[13] C.T. Lee, W.T. Yang, R.G. Parr, Phys. Rev. B 37 (1988) 785.
[14] S.H. Vosko, L. Wilk, M Nusair, Can. J. Phys. 58 (1980) 1200.
[15] P. Csaszar, P. Pulay, J. Mol. Struct. (THEOCHEM) 114 (1984) 31.
[16] J. H. Schachtschneider, Technical Report; Shell Development Co. Emeryville, CA, 1969.
[17] C. Peng, H.B. Schlegel, Israel J. Chem. 33 (1994) 449.
[18] J. Herzig, J. Pollak, J. Monatsch. Chem. 29 (1908) 263.
[19] R. Wegschneidler, H. Gehringer, J. Monatsch. Chem. 29 (1909) 529.
[20] L. Bouveault, R. Locquin, Bull. Soc. Chim. Fr. 5 (1910) 1136.
[21] I.D. Reva, S. Stepanian, L. Adamowicz, R. Fausto, J. Phys. Chem. A 105 (2001) 4773.
[22] I.D. Reva, S.G. Stepanian, L. Adamowicz, R. Fausto, Chem. Phys. Lett. 374 (2003) 631.
[23] A. Kulbida, R. Fausto, J. Chem. Soc. Faraday Trans. 89 (1993) 4257.